CCFE
CULHAM CENTRE FOR FUSION ENERGY

UK Atomic Energy Authority

UKAEA-CCFE-PR(22)50

Nick Walkden, Fabio Riva, James Harrison, Fulvio Militello, Tom Farley, John Omotani

Origin, drive and characteristics of turbulence in the divertor volume of the Mega Amp Spherical Tokamak

Origin, drive and characteristics of turbulence in the divertor volume of the Mega Amp Spherical Tokamak

Nick Walkden, Fabio Riva, James Harrison, Fulvio Militello, Tom Farley, John Omotani

The physics of turbulence localised to the tokamak divertor volume

N.R.Walkden, F.Riva, J.Harrison, F.Militello, T.Farley, and J.T.Omotani

CCFE/UKAEA, Culham Science Center, Abingdon, Oxfordshire, OX14 3DB, UK

B.Lipschultz

York Plasma Institute, Dept. Physics, Univ. York, Heslington, York, YO10 5DD, UK

Fusion can only be viable as a future sustainable energy source if heat and particles generated in the fusion plasma can be safely exhausted without inflicting performance limiting damage. Fusion power plant designs based on magnetic confinement, such as the tokamak design, offer a promising route to sustainable fusion power but require robust exhaust solutions capable of tolerating intense heat and particle fluxes from the plasma at the core of the device. Turbulent plasma transport in the region where the interface between the plasma and the materials of the device is handled - called the divertor volume - is poorly understood, yet impacts several key factors ultimately affecting device performance. In this letter a comprehensive study of the underlying physics of turbulence in the divertor volume is conducted using data collected in the final experimental campaign of the MAST device producing two-dimensional maps of turbulent flows in the divertor volume, compared to high fidelity nonlinear simulations. The physics of the turbulence is shown to be strongly dependant on the geometry of the divertor volume - a potentially important result as the community looks to advanced divertor designs with complex geometry for future fusion power plants. These results lay the foundations of a first-principles physics basis for turbulent transport in the tokamak divertor, providing a critical step towards a predictive understanding of tokamak divertor plasma solutions, which in turn will drive the design of future fusion power plants.

Introduction

Fusion offers the potential of abundant, carbon-free, agile, baseload energy supply to complement renewable generation and meet energy demand in the post-carbon era. The fusion process both requires and generates heat in abundance. A commercially viable fusion plant must be sufficiently available to produce cost-effective energy, which in turn requires that any excess heat and particles arising from the fusion plasma must be exhausted without causing perfomance limiting damage to the device. This is a well known and severe challenge given the scale of the heat flux expected from a burning fusion plasma. Successful deployment of fusion energy is thus contingent on a solution to the challenge of plasma exhaust, which demands a sound understanding of the transport processes within the exhaust volume of the device, called the divertor. This paper reports new results, developed through a combination of advanced measurement - including fully two-dimensional turbulent flow maps in the divertor volume - and state-of-the-art simulation, that represent a step-change in the knowledge base of key turbulent transport processes that occur in the divertor. These results lead to the statement of a simple theory regarding the impact of the geometry of the divertor system on turbulent transport; A timely contribution as fusion power plant designs increase focus on 'advanced' divertors with modified geometry [1], and the new device MAST Upgrade finishes its first experimental campaign to investigate such designs.

The divertor volume exists below the X-point of tokamak plasmas. The X-point is a null in the poloidal magnetic field that separates the hot core plasma, where magnetic field lines are closed, from walls of the device via a thin external layer of open ended magnetic field lines called the 'scrape-off layer'. The scrape-off layer acts as a channel of heat and particles to material surfaces down the divertor 'legs'. The intensity of plasma transport to material surfaces in the divertor influences the design of tokamak based fusion reactors such as ITER [2, 3], DEMO [4], or the UK STEP[5] design. Indeed in fusion power plants the challenge of successfully exhausting excess heat from the fusion process, and particles including both unspent fuel and helium, is such that conventional divertors may be insufficient and 'advanced' divertors are a key area of development for the international community [1]. Advanced divertors generally rely on a modification of the geometry of the divertor legs to realise favorable impacts [6]; an example is the Super-X divertor, where the divertor leg is extended to a greater radial location spreading the heat and particles over a larger area and allowing more time for the plasma to cool, which is being tested on the new device MAST Upgrade [7].

Turbulence within the plasma is commonplace in the edge and SOL regions where severe thermodynamic gradients build up in the plane perpendicular to the magnetic field, and impacts on the performance of the divertor system. Turbulent processes from the hot-core eject plasma into the scrape-off layer (SOL) in discrete structures often called filaments or blobs [8], which then flow parallel to the magnetic field into the divertor volume. Thermodynamic gradients built up inside the divertor volume in turn provide free energy for localised turbulent transport to redistribute heat and particles deeper into the SOL, or into the private-flux region (PFR) - the region between divertor legs that is un-connected to the upstream plasma. These processes are described schematically in figure 1.

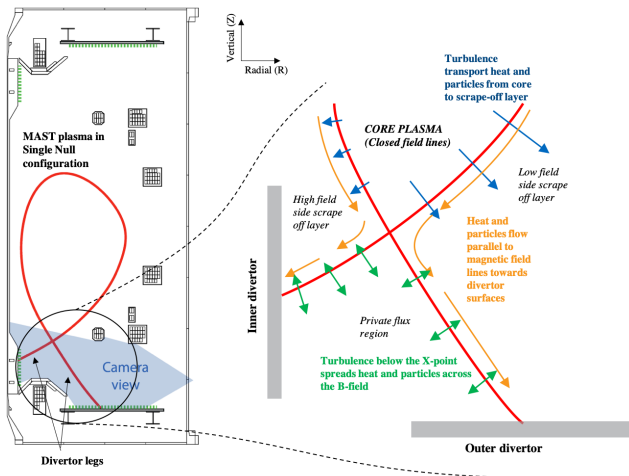Divertor localised turbulent transport has been sparsely

FIG. 1. Schematic illustration of turbulent and parallel transport processes in the divertor volume which exists below the X-point in a tokamak plasma. Turbulence in the hot core ejects particles and heat into the scrape-off later (blue arrows) which flows along magnetic field lines into the divertor volume (orange arrows), to be re-distributed into the SOL and PFR (green arrows) in divertor legs before intersection with material surfaces.

studied, yet can have a significant impact on the performance of the device and longevity of divertor components through factors including:

- The onset of divertor detachment, a highly radiating state that cools plasma in advance of the material interface;

- the peak divertor ion temperature which is a critical parameter determining the sputtering of the material surface;

- and, the peak heat-flux to the divertor target which crucially determines the potential for surface melting and damage.

Indeed, the effect of turbulent transport in the divertor must be accounted for heuristically to correctly interpret the profile of the heat flux observed to impinge on divertor surfaces in present day devices (accounted for in the S parameter of the commonly used 'Eich' fitting function for thermographic measurements of divertor surface heat fluxes) [9]. Laminar simulations, often the tool of choice to interpret edge and divertor physics in present day experiments, and to design future ones, employ ad-hoc transport coefficients to capture this effect which do not account for any dependance of turbulent transport on the geometry of the divertor configuration. The scale of the transport that must be set in laminar simulations to match experiments is anomalously high, and cannot be accounted for by collisional transport processes. As such, setting a physics basis for turbulence in the divertor volume is important both for present day

interpretation and predictive design of future devices, particularly those with advanced divertors. This letter combines advances in experimental data analysis and turbulence model development to enable the first major study of the physics underlying localised transport in the divertor volume. The results of this work provide the foundations of a first-principles physics basis ultimately needed for full predictability of the overall divertor plasma solution and performance, and demonstrates a leading order impact of the divertor geometry on turbulent transport levels.

Methodology
Despite a relative sparsity of literature concerning the physics of divertor localised turbulence, there exists a significant and growing empirical basis. High speed imaging is a commonplace technique used to analyse turbulence in the tokamak boundary, and has revealed turbulent structures in the divertor volume of tokamak devices including NSTX [10, 11], Alcator C-Mod [12, 13], TCV [14] and MAST [15–18]. Concurrently, advanced tomographic inversion methods for 3D structures in high speed imaging data [19, 20] have been developed to allow deeper analysis of this complex imaging data. The method developed and deployed in this paper is described and rigorously tested by Farley et al. [20, 21] and provides a mapping between the complex image recorded by a high speed camera and a two-dimensional plane in the divertor, taken here as the poloidal (radial-vertical) plane around the inner and outer divertor legs, by assuming that the 3D structures being imaged by the camera align to the background magnetic field (an assumption that is confirmed in simulation). This allows for the formation of a basis on which to perform a tomographic inversion. During the pre-processing stage, subtraction of the pixel-wise minimum of a given frame with its 19 predecessors [22, 23] is applied to isolate fluctuations from the slowly-varying background component of the light. Figure 2 a), b) and d) show an example of a typical camera frame with important features of the plasma indicated. The effect of background subtraction on that frame is shown in panel b), and the inversion of the background subtracted image onto the inner and outer divertor legs is shown in panel d). The inversion domain is chosen to isolate the private-flux region (PFR) and near scrape-off layer (SOL) region of both divertor legs, avoiding the X-point and core plasma. The light emission contained in the camera images which are central to this analysis are dominated by Balmer $3 \Rightarrow 2$ emission and are a complex nonlinear function of plasma quantities - density, temperature and neutral density. Without a multi-measurement comparison, which is extremely challenging for turbulent structures and was not practicable for MAST, the direct experimental inference of these thermodynamic quantities and (more importantly) their fluctuations utilising the diagnostic camera images could not be carried out, though previous studies indicate consistency between camera and probe

fluctuation measurements [16, 18]. Instead, this study utilizes the turbulence code (STORM) for predictions of the plasma turbulent solution to forward model the Balmer $3 \Rightarrow 2$ light emission observed in synthetic camera image measurements. This provides like-for-like comparison of experiment and simulation, ensuring that any systematic uncertainties are respected in both datasets and allowing high-level comparisons and conclusions to be drawn with confidence.

The STORM module [25, 26] of the BOUT++ framework [27, 28] produces high fidelity simulations of tokamak boundary turbulence and has recently been validated against experimental measurements of the motion of individual turbulent structures [29] and separately against full scale turbulence [24] in the upstream region (immediately adjacent to the core plasma) of the MAST device. This paper employs synthetic images of the divertor turbulence derived from simulations conducted by Riva et al.[24]: Data from the the simulation is interpolated onto a grid identical to that used in the experimental analysis, which is then projected along the path of the magnetic field to produce a camera image accounting for line-integration effects and occlusion by machine structures. The emissivity in the poloidal plane is a complex function of thermodynamic quantities of the plasma and neutral gas, and atomic physics, and is forward-modelled in this paper using the OpenADAS database [30] for the Balmer $3 \rightarrow 2$ transition, employing a neutral particle distribution from a complementary laminar simulation including plasma-neutral interactions. The frames are then processed in the same manner as the experimental data. A synthetic camera frame is shown in figure 2 c). By design the image does not account for any emission from the X-point, core plasma or outer-SOL regions to capture only the salient features of the divertor legs allowing for robust comparison between simulation and experiment.

Experimental database
This paper focusses on results from the spherical tokamak device, MAST [31], during it's final experimental campaign in 2013. During these experiments a visible light camera capable of recording in excess of 120,000 frames per second was placed on the divertor with a tangential view into the vessel (see figure 1) for several hundred individual plasma discharges. Rather than base this study on individual plasma discharges within this set, a database has been drawn together that covers the widest available parameter range of the plasmas viewed by the camera. Plasma parameters from the database are given in table I. The database is constructed of discharges mainly configured in the lower single null (LSN, where only the lower X-point is active) configuration (pictured in figure 1) where the data quality is highest, but also considers the impact of resonant magnetic perturbations (used to control violent edge instabilities) and High confinement (H-) mode. The STORM simulation analysed is in the slightly

different 'lower disconnected double null configuration', where both X-points are active, but the lower is still the primary X-point. From the perspective of the near SOL and PFR of the lower divertor, the STORM simulation is comparable to a LSN plasma and is therefore a reasonable choice for this study. By considering a wide database of discharges, it will be shown that properties of divertor turbulence are reasonably insensitive to plasma parameters as measurements made tend to cluster, which in turn strengthens confidence in high-level conclusions drawn. The strategy employed in this paper is to compare simulation and experiment with robust measurements to draw high-level conclusions around the characteristics of the turbulence, and importantly to validate these aspects of the simulations. With the simulations validated, the flexibility of the code will be leveraged to diagnose the fundamental physics drivers of the turbulence.

Results: Shape and distribution of turbulent structures
Turbulence is complex and difficult to diagnose with acceptable uncertainty. In order to draw robust conclusions, this paper focusses on simple and robust measurements that can be readily compared between divertor legs, and between experiment and simulation. The first such set of measurements forms an assessment of the shape and distribution of turbulence structures across the database by calculating a quasi toroidal mode-number (the number of structures in 2π radians toroidally around the device), calculated by counting peaks in the emission along the projection of a magnetic field line in the R-Z plane, and the poloidal structure width calculated as the full-width half maximum of these identified peaks. A useful radial coordinate is the 'poloidal magnetic flux' normalised using values at the magnetic axis ψ_{ax} and separatrix ψ_{sep}, such that $\psi_N = (\psi - \psi_{\mathrm{ax}})/(\psi_{\mathrm{ax}} - \psi_{\mathrm{sep}})$. The analysis is carried out on the flux surface at $\psi_N = 0.99$ which is sufficiently far into the PFR to avoid questions of magnetic field reconstruction misalignment, but sufficiently close to the separatrix that the flux of turbulent structures across the surface is significant. A systematic offset of the experimental flux-surfaces is present which results in a radial shift of measurements by $\Delta\psi_N = 0.005$, though this has little impact on the conclusions of this study. In figure 2 d) the embedded white lines show the trajectory of the $\psi_N = 0.99$ surface in the R-Z plane in the inner and outer divertor legs, and in e) the emissivity along the surface is shown in an example discharge. This is cast onto the toroidal angle subtended by the analysed section of the magnetic field line simply by mapping the projection of the magnetic field. By casting this data onto the toroidal angle it is possible to directly compare the features of the inner and outer legs. Fewer peaks are detected per radian of toroidal angle in the inner PFR than in the outer. If turbulent structures in one leg where connected (along magnetic field lines)
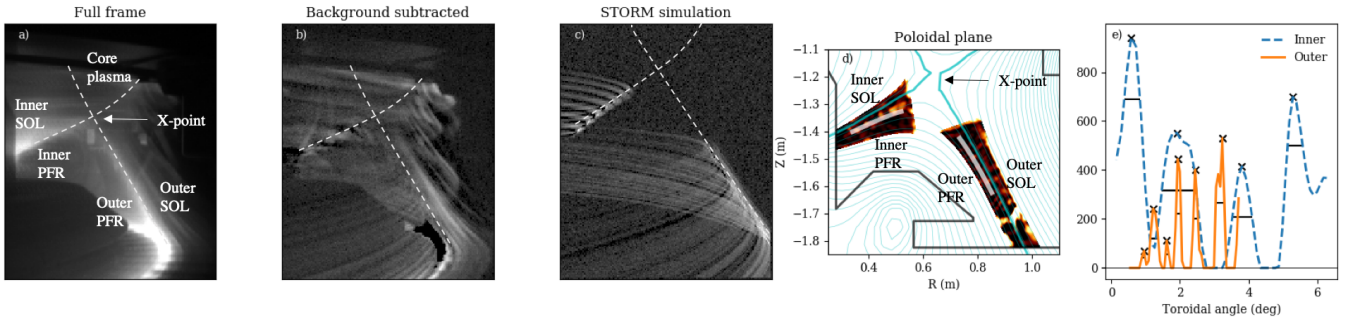
FIG. 2. Example of the typical process for data analysed in this paper. a) and b) raw and background subtracted camera data. c) Synthetic camera data from the STORM simulation (see ref [24] for simulation details). d) Tomographically inverted data on sections of the poloidal plane around the inner and outer divertor legs. White lines indicate line-segments where the emissivity is extracted for analysis in e), the inverted emissivity from the line segments in panel d projected onto the toroidal angle on the $\psi_N = 0.99$ flux surface. Crosses mark detected peak locations, horizontal lines show local FWHM.

Discharge	Confinement Mode	$n_{e,sep}(10^{19}m^{-3})$	$T_{e,sep}(eV)$	$I_p(MA)$	$B_{tor}(T)$	$P_{NBI}(MW)$
29606	L-mode	0.72	18	0.63	-0.59	0
29608	L-mode	0.97	17	0.63	-0.57	0
29651	L-mode	0.85	24	0.62	-0.55	1.27
29660	L-mode (RMPs)	0.94	25	0.63	-0.54	1.22
29668	L-mode	1.05	27	0.63	-0.56	0.61
29669	L-mode	1.25	19	0.42	-0.51	0.62
29693	L-mode	0.97	32	0.42	-0.48	1.23
29718	L-mode	1.00	38	0.63	-0.54	1.61
29720	L-mode	1.37	29	0.42	-0.47	1.61
29723	H-mode (ELM-free)	1.4	55	0.82	-0.56	1.6
STORM [24]	L-mode	0.5	15	0.4	-0.4	0

TABLE I. Survey of plasma parameters from MAST for experimental analysis, alongside the simulation carried out in the STORM code. The database covers a wide range of parameter including: High and low confinement mode; plasma density and electron temperature (measured at the upstream separatrix); plasma current; toroidal magnetic field; and, input heating power.

to the other, then this mode number would necessarily be equal in both - the clear difference therefore demonstrates that turbulent structures in the inner and outer divertor legs are isolated from one another. Figure 3, which accumulates these measurements across the entire database as a histogram, demonstrates that this result holds consistently with a clear separation in the PDFs of the quasi toroidal mode number between inner and outer divertor legs. This corroborates measurements made on specific discharges in the NSTX device (a sister spherical tokamak to MAST) [11], and demonstrates that this feature is ubiquitous to divertor turbulence (at least in spherical tokamaks). The simulation reflects the qualitative trend found in experiment, with a significant difference in mode numbers measured in the inner and outer legs, with a well reproduced toroidal mode number distribution in the inner divertor leg, however a tendency towards higher mode numbers in the outer divertor leg is present, possibly indicating higher wavenumber turbulence generated in the simulation. Also shown in figure 3, the poloidal filament widths in both inner and outer legs are similar and the simulation faithfully reproduces the scale of turbulent structures
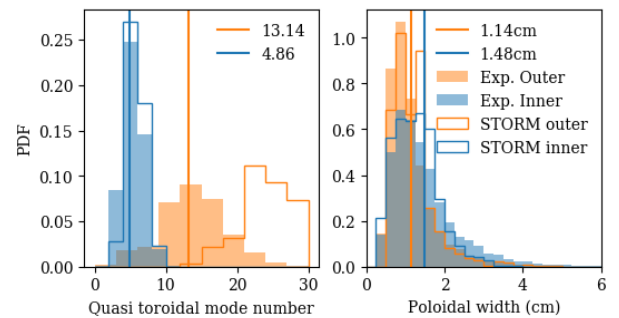

FIG. 3. (Left) Quasi-toroidal mode number and (Right) poloidal FWHM cumulative distributions across all discharged detailed in table I. Mean values are represented by vertical lines. Data from the simulation [24] is shown as solid lines, whilst experimental data as filled histograms. The clear separation in the PDFs of toroidal mode number between inner and outer legs demonstrate conclusively that turbulence in the two legs is independant.

derived from experimental measurements. Despite both divertor legs showing similar real-space widths,

the variation in magnetic field strength from inner to outer leg means that, relative to the Larmor radius, $\rho_s = \sqrt{T_e m_i}/eB$ ($\approx 0.5mm$ for the inner and $\approx 1mm$ for the outer), the inner-leg structures are $2-3$ times larger than the outer leg. In both measurements made, it is notable that the individual PDFs from each discharge (omitted from Fig. 2 for clarity) match closely the cumulative PDFs shown in Fig. 2, indicating that the observations made are insensitive to the parameters of the plasma within the range of parameters considered (which largely cover the range available) and are thus reasonably considered fundamental to the properties of the turbulence observed in the MAST divertor. This is true even for a comparison between L-mode and H-mode, though note that the H-mode studied here is the more exotic ELM-free state, used so that sufficient statistics could be generated without ELM events contaminating the measurement. The spectral characteristics of the turbulence were also investigated on the same flux surface from tomographically inverted experimental and simulation data, and demonstrated poloidal wavenumbers in the range $|k_\theta|\rho_s < 0.4$ for the outer divertor leg and $|k_\theta|\rho_s < 0.2$ for the inner across a broad frequency band up to and above $40kHz$. These spectra are shown in figure 4. Again, measurements in
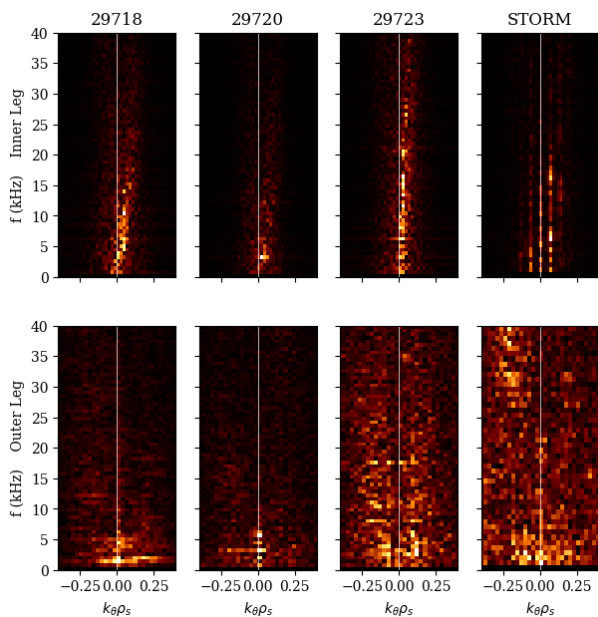

FIG. 4. Wavenumber (relative to larmor radius) and frequency spectra from the $\psi_N = 0.99$ surface from the inner (top) and outer (bottom) divertor legs. Three experimental examples are provided from the database outlined in table I alongside the simulation.

simulation and experiment are consistent (noting a more modal behaviour in the simulation which is due to a toroidally periodic domain with a period of πradians). The condition of $k_\theta\rho_s < 1$ is well satisfied in both divertor legs, which is a key condition for the application

of drift-reduced fluid models [32] such as that used in the STORM model that the simulations considered here are based on. This indicates that the class of model used in simulatons here can be considered reasonable for turbulence localised to the divertor volume.

Results: Flows
Since the novel tomographic inversion employed in this paper produces 2D time-histories in the R-Z plane, flow velocities can be derived by mapping the trajectory of turbulent structures. To this effect, velocimetry based on two-point time-delayed cross-correlations has been used here to map the average flow of structures in the inner divertor leg (no clear directive flow was reliably measurable in the outer divertor leg, as demonstrated in figure 4). This technique produces a full 2D map of the time-averaged flow of turbulent structures, an example of which is given in figure 5 (upper panel). The features in this example are typical to all shots analysed, and show structures moving dominantly poloidally (along the projection of magnetic field lines, the θ direction) near to the separatrix but dominantly radially (the ψ_N direction) deeper into the PFR. To compare the flows across the database, the vectors are decomposed into directions parallel to and perpendicular to the projected magnetic field lines and averaged. The discharges with plasma current of $Ip = 400kA$, which matches the conditions used for the STORM simulation, are highlighted in blue. There is a net flow of turbulent structures in both the radial and poloidal directions that exhibits broadly similar behavior across the database. Near to the separatrix, the flow measured in the inner leg is directed poloidally towards the divertor target but transitions to a radial flow in the far PFR. The profiles and magnitudes of the flow measured in the simulation match that of the experimental dataset well in the vicinity of the separatrix but the radial flow is suppressed in the far PFR suggesting that the transport level in the simulation may be an under-estimation of experiment. In the deep PFR turbulent structures in the simulaton are observed to decay within the inter-frame time of the synthetic movie and are therefore not trackable by the velocimetry which is based on frame-to-frame correlations, indicating that losses in the simulation (dominantly parallel losses) may be exaggerated compared to experiment. The poloidal flow is directed towards the target in the PFR and away from the target in the SOL of the inner divertor leg. Taking $v_\theta \sim 0.5km/s$ from figure 5, and reasonable estimates of $n_e \sim 0.6 \times 10^{19}m^{-3}$ and $T_e = T_i = 20eV$ for the electron density and electron/ion temperature respectively, gives a convected heat flux of $0.05MW/m^2$ towards the target. This is around 25% of the typical heat flux measured at the MAST inner target ($0.2MW/m^2$ as measured in ref [33]) indicating that the contribution of poloidal cross-field flows to target heat fluxes in MAST may be significant. Interrogation of the simulations reveals that the poloidal flow of turbulent structures
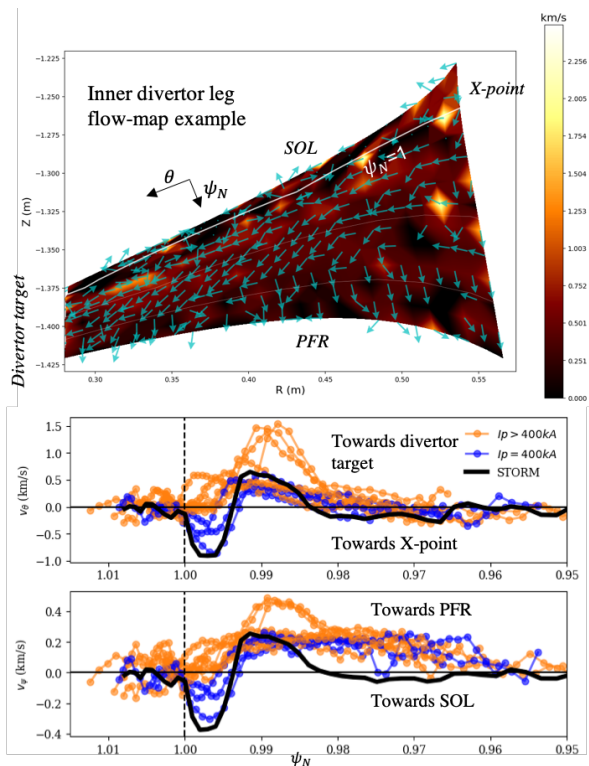
FIG. 5. Upper: Example flow map measured in the inner divertor leg of an example discharge. Lower: Poloidal (θ) and radial (ψ_N) flows in the inner divertor leg averaged poloidally for all plasmas in the database. Blue traces indicate plasmas with $I_p = 400kA$ (matching conditions used for the STORM simulation) whilst orange traces indicate plasmas with $I_p > 400kA$.

is likely an entrainment in the $\mathbf{E} \times \mathbf{B}$ flow due to the sheath potential, whilst the radial flow is due to the cross-field propulsion of turbulent structures.

Results: Turbulence drives

Within this paper, reasonable agreement between the nonlinear fully turbulent STORM simulation and measurements across the MAST experimental database is demonstrated both qualitatively and quantitatively (within 30% in most instances). There are notable over estimates in the STORM toroidal mode number in the outer divertor leg, and underestimates in the radial transport into the far PFR of the inner leg, however the leading order details of the turbulence are well reproduced. On this basis, the simulation can be tentatively used to diagnose the origin and drive of the turbulence, a key first step towards establishing a first-principles understanding of the transport. A simulation study has been carried out in the manner of Ricci and Rogers [34, 35] by eliminating terms from the vorticity equation, which determines the electrostatic potential and therefore regulates turbulence, that are known to drive certain classes of turbulent trasport. The

vorticity equation in STORM is [24]

$$\frac{\partial \Omega}{\partial t} + U\mathbf{b} \cdot \nabla\Omega = -\frac{1}{B}\mathbf{b} \times \nabla\phi \cdot \nabla\Omega + \frac{1}{n}\nabla \times \left(\frac{\mathbf{b}}{B}\right) \cdot \nabla P$$

$$+\frac{1}{n}\nabla \cdot \left(\mathbf{b}J_{||}\right) + \mu_{\Omega_0}\nabla_\perp^2\Omega \qquad (1)$$

where ϕ is the plasma potential, $\Omega = \nabla \cdot (B^{-2}\nabla_\perp\phi)$ the scalar vorticity, B the magnetic field strength, $P = nT$ the electron pressure, n and T the electron density and temperature, $J_{||} = n(U - V)$ the parallel current with U and V the ion and electron velocities parallel to the magnetic field, $\mathbf{b}$ the magnetic field unit vector and μ_Ω the (small) collisional perpendicular viscosity. This equation has three terms that drive different classes of turbulence. The term $\frac{1}{n}\nabla \times \left(\frac{\mathbf{b}}{B}\right) \cdot \nabla P$ drives interchange turbulence [36], which is analogous to Rayleigh-Taylor turbulence, and is driven by thermodynamic gradients in regions where the curvature of the magnetic field has a destabilising effect. The term $\frac{1}{B}\mathbf{b} \times \nabla\phi \cdot \nabla\Omega$ drives Kelvin-Helmholtz turbulence via sheared flows [37], whilst the term $\frac{1}{n}\nabla \cdot \left(\mathbf{b}J_{||}\right)$ term mediates drift-wave turbulence driven ubiquitously by cross-field thermodynamic gradients in a resistive plasma. To test the effect of these three different mechanisms, three simulations were performed beginning from the baseline simulation presented in this paper thus far, with the three turbulent drive terms removed in turn. To remove interchange turbulence from the simulation, $\nabla \times \left(\frac{\mathbf{b}}{B}\right) \to 0$ was set in the lower divertor. To remove Kelvin-Helmholtz turbulence, $\mathbf{b} \times \nabla\phi \cdot \nabla\Omega \to< \mathbf{b} \times \nabla\phi \cdot \nabla\Omega >_\Phi$ in the vorticity equation, whilst to remove drift-waves the substitution $\frac{1}{n}\nabla_{||}P \to< \frac{1}{n}\nabla_{||}P >_\Phi$ is made in parallel Ohm's law (equation 4 from ref [24]) which blocks energy transfer into resistive drift-waves. $<>_\Phi$ indicates a toroidal average in the divertor volume. Figure 6 compares the poloidally averaged turbulent cross-field heat flux for each of these cases with the full simulation in each divertor leg. In interpreting figure 6, the reader should compare each coloured line in turn to the black line to infer the effect of each of the classes of turbulence. Turbulence in the inner divertor leg spreads heat more effectively into the PFR than in the outer, consistent with thermographic measurements made by Militello *et al* [33]. This is demonstrated qualitatively in the cross-section from the simulation, shown in the upper panel of figure 6, where significantly more turbulence activity can be seen in the inner divertor leg than the outer. The nature of the turbulence in the PFR of the inner-leg can be classed drift-interchange, with a clear reduction in the heat-flux occurring when either resistive drift-waves or interchange turbulence is removed from the system. KH turbulence is not a driver, but close to the separatrix shear-flow effects are stabilising as their removal leads to higher transport fluxes. The inner-leg PFR is a 'bad-curvature' region, where thermodynamic gradients are parallel to the curvature vector of the magnetic
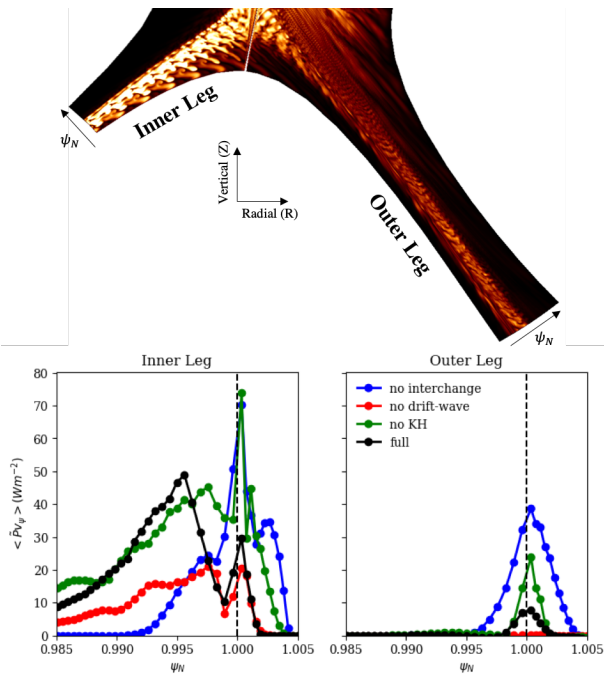
FIG. 6. Poloidally averaged turbulent radial heat fluxes into the PFR in STORM simulations of MAST [24] in the inner and outer divertor legs. Fluxes are compared between the full simulation (black) and simulations with interchange (blue), drift-wave (red) and Kelvin-Helmholtz (green) turbulence removed respectively. A positive flux indicates transport into the PFR.

field, and is analogous to the low-field side SOL. In bad-curvature regions magnetic curvature drives turbulence, as demonstrated by figure 6. By contrast, the outer-leg PFR is a 'good-curvature' region and the removal of interchange effects leads to a dramatic increase in the radial heat flux (directed into the PFR). Once again in the outer divertor leg KH instabilities are not present and shear flows are stabilising near the separatrix. The turbulence in the outer leg arises entirely from unstable drift-waves, the removal of which completely suppresses radial heat transport into the PFR and the turbulence may be classed as drift-wave turbulence. For like-for-like conditions, the difference in turbulence between inner and outer legs implies that the inner leg will exhibit enhanced transport into the PFR compared to the outer - an effect that is rarely if ever represented in ad-hoc transport used in laminar modelling of the divertor. It is notable that this effect relies only on the geometry of the divertor legs, so is likely to be ever-present other than for deeply exotic configurations. The important and contrasting role of the magnetic curvature demonstrates that it is a leading order actuator to vary turbulence levels in divertor legs. This statement allows for the postulation of a simple theory: The orientation of a divertor leg in the poloidal plane has a leading order impact on the level of localised transport due to divertor turbulence. The effect (stabilising or destabilising) of

the magnetic curvature is maximised when a divertor leg is vertical, since thermodynamic cross-field gradients are fully parallel/anti-parallel to the curvature vector. Conversely the effect of magnetic curvature is minimised in a horizontal divertor leg. In principle the effects described would be opposite in the SOL where gradients are respectively reversed, however light levels in the inner leg SOL prevent any measurement of turbulence there and the outer leg SOL is dominated by turbulence originating above the X-point, so there is not sufficient basis to make statements about these regions. Drift-wave turbulence is everpresent, however the impact of magnetic curvature can enhance/suppress the turbulence level. This means that transport is maximised in the inner divertor leg when it is angled normal to the radial direction because the *destabilising* effect of magnetic curvature enhances transport. Transport is maximised in the outer divertor leg when it is angled horizontally (parallel to the radial direction) because the *stabilising* effect of the magnetic curvature is minimised. This is potentially important for the understanding of future power-plant divertor designs, where advanced concepts such as the 'Super-X' divertor[38–40] are being considered which is characterised by a long, near radial divertor leg. The Super-X divertor is being prototyped on MAST Upgrade[7], with a long radial divertor leg that is exceptionally well diagnosed. The results presented in this paper imply that such a configuration should maximise the rate of turbulent transport in the outer divertor leg; a potentially testable hypothesis. Moreover, all of the effects discussed are likely to present strongest in tight aspect ratio devices due to their reduced major radius and, therefore, increased magnetic curvature.

Summary

In summary this letter combines advanced measurement techniques of high speed camera footage, a novel tomographic reconstruction method, and high fidelity turbulence simulations to assess the physics of localised turbulence in the divertor volume of MAST. The simulations reproduce the spectral characteristics, size, distribution, and flow of turbulent structures within the divertor volume. These characteristics are found to be largely invariant across a wide experimental dataset indicating that divertor turbulence is insensitive to operational parameters. Turbulence in the two divertor legs is decoupled and radial heat transport in the inner divertor is stronger than in the outer due to the effects of magnetic curvature. The validated simulations demonstrate that unstable resistive drift-waves contribute to turbulence in both divertor legs. Magnetic curvature further destabilises the inner divertor leg and the turbulence is therefore classified as drift-interchange, whilst it has a stabilising effect in the outer leg where the turbulence is classified as drift-wave. This theoretical finding indicates that modification of divertor leg geometry may offer a route towards optimising turbulent transport in the divertor. This work provides a comprehensive foun-

dation for a first-principles understanding of turbulence in the divertor, which is a critical step towards a fully predictive capability for tokamak divertor performance which in turn will drive the design of future fusion power plants. The new MAST Upgrade device, which is has now finished its first experimental campaign, is ideally positioned to test this theory in coming years.

[1] H.Zohm *et al.*, Fusion Engineering and Design **166**, 166 (2021).

[2] A.Loarte *et al.*, Nuclear Fusion **47**, S203 (2007).

[3] R.A.Pitts *et al.*, Physica Scripta **T138**, 014001 (2009).

[4] R.Wenninger *et al.*, Nuclear Fusion **55**, 063003 (2015).

[5] Nature, https://doi.org/10.1038/d41586-019-03039-9 (2019).

[6] M. Kotschenreuther *et al.*, Physics of Plasmas **20**, 102507 (2013).

[7] W.Morris *et al.*, IEEE Transactions on Plasma Science **46**, 5 (2019).

[8] D. A. D'Ippolito, J. R. Myra, and S. J. Zweben, Physics of Plasmas **18**, 060501 (2011).

[9] T. Eich *et al.*, Physical Review Letters **107**, 215001 (2011).

[10] R.J.Maqueda, D.P.Stotler, and the NSTX Team, Nuclear Fusion **50**, 075002 (2010).

[11] F.Scotti *et al.*, Nuclear Fusion **58**, 126028 (2018).

[12] J.L.Terry *et al.*, Nuclear Materials and Energy **12**, 989 (2017).

[13] S.B.Ballinger *et al.*, Nuclear Materials and Energy **17**, 269 (2018).

[14] N.R.Walkden *et al.*, Plasma Physics and Controlled Fusion **60**, 115008 (2018).

[15] J.R.Harrison, G.M.Fishpool, and B.D.Dudson, Journal of Nuclear Materials **463**, 757 (2015).

[16] J.R.Harrison *et al.*, Physics of Plasmas **22**, 092508 (2015).

[17] N.R.Walkden *et al.*, Nuclear Materials and Energy **12**, 175 (2017).

[18] N.R.Walkden *et al.*, Nuclear Fusion **57**, 126028 (2017).

[19] J.Cavalier *et al.*, Nuclear Fusion **59**, 056025 (2019).

[20] T.Farley *et al.*, Review of Scientific Instruments **90**, 093502 (2019).

[21] T.Farley, PhD Thesis, Univ. Liverpool (2020).

[22] B. D. Dudson *et al.*, Plasma Physics and Controlled Fusion **50**, 124012 (2008).

[23] N. B. Ayed *et al.*, Plasma Physics and Controlled Fusion **51**, 035016 (2009).

[24] F.Riva *et al.*, Plasma Physics and Controlled Fusion **61**, 095013 (2019).

[25] L. Easy *et al.*, Physics of Plasmas **21**, 122515 (2014).

[26] N.R.Walkden, L.Easy, F.Militello, and J.T.Omotani, Plasma Physics and Controlled Fusion **58**, 115010 (2016).

[27] B. D. Dudson *et al.*, Computer Physics Communications **180**, 1467 (2009).

[28] B. D. Dudson *et al.*, Journal of Plasma Physics **81**, 365810104 (2015).

[29] F.Militello *et al.*, Plasma Physics and Controlled Fusion **58**, 105002 (2016).

[30] H.P.Summers, The ADAS User Manual, version 2.6 http://www.adas.ac.uk (2004).

[31] A. Sykes *et al.*, Nuclear Fusion **41**, 1423 (2001).

[32] A. N. Simakov and P. J. Catto, Physics of Plasmas **10**, 4744 (2003).

[33] F.Militello *et al.*, Nuclear Fusion **56**, 016006 (2015).

[34] P.Ricci and B.N.Rogers, Physical Review Letters **104**, 145001 (2010).

[35] B.N.Rogers and P.Ricci, Physical Review Letters **104**, 225002 (2010).

[36] O. E. Garcia, V. Naulin, A. H. Nielsen, and J. J. Rasmussen, Physics of Plasmas **12**, 062309 (2005).

[37] K.Lotov, D.Ryutov, and J.Wieland, Physica Scritpa **50**, 153 (1994).

[38] P. M. Valanju, M. Kotschenreuther, S. M. Mahajan, and J. Canik, Physics of Plasmas **16**, 056110 (2009).

[39] I. Katramados *et al.*, Fusion Engineering and Design **86**, 1595 (2011).

[40] G. Fishpool *et al.*, Journal of Nuclear Materials **438**, S356 (2013).